Biomechanical Characterization of the Atherosclerotic Burden in Genetically Modified Mice

with a special focus on the

Roles of Thrombus and Collagen Remodeling in Intramural Healing of Dissecting Aortic Aneurysms

A FINAL REPORT TO THE AUSTRIAN MARSHALL PLAN FOUNDATION

by

D.I. ANDREAS JÖRG SCHRIEFL

for receiving funding for a Visiting Assistant in Research position
from June – September 2011 at the

Biomedical Engineering Faculty
at the
Yale School of Engineering & Applied Science

Graz, Austria, November 2011

TABLE OF CONTENTS

PREFACE

Doing research for four months at the Yale School of Engineering & Science was a very positive experience on many different levels. Scientifically it allowed me to work in an environment of world renowned scientists which naturally was an eye-opening experience and will be beneficial not only to myself but also to the Institute of Biomechanics at the Graz University of Technology. For example, some of the newly gained knowledge from my stay at Yale University can also be utilized in our laboratory in Graz and will play an important role in future research projects. Culturally, living in the United States for an extended period of time gave me not only insight into differences in the way of life outside the University environment compared to Austria, but also let me observe differences in organization and management within the University system compared to the TU Graz, therefore, adding another interesting layer to this entire experience abroad.

As for the content of this final report I decided to present the key findings in a paper-like structure. Other important work which took up a significant amount of time but will not be part of the paper that we are planning to publish is included in the appendix. Specifically supplemental figures and background information on histological stains can be found there (mostly obtained through internet research), which guided our decision making process on which stains were most fitted for our purposes.

Graz, Austria, November 2011 *Andreas J. Schriefl*

ACKNOWLEDGEMENTS

None of this would have been possible without the very kind and generous invitation from Prof. Jay D. Humphrey, Professor of Biomedical Engineering at the Yale School of Engineering & Applied Science, Yale University, CT, USA. He not only guided me scientifically throughout my entire stay at Yale University but was also of much help during the preparation process involving many bureaucratic hurdles. Upon arrival he provided me with a comfortable office space, state of the art computer and laboratory equipment and most importantly, tissue samples from ANG-II deficient mice prepared by his former PhD students.

A special thanks also goes to Prof. Laura E. Niklason, Professor of Anesthesiology & Biomedical Engineering at Yale University for her valuable input during the histological analysis of intramural thrombi.

Next I would like to thank my colleagues at the Biomechanics Lab at Yale for all their help and assistance, namely John Wilson, Jacopo Ferruzzi, David D. Simon, Paolo Diachille, Yongung Lee and Katia Genovese.

In Austria I owe gratitude to my PhD advisor, Prof. Gerhard A. Holzapfel, for his support in getting this project started and allowing me to do research away from my home institution for a not insignificant period of time.

Last but not least I would like to thank Karin Leber from the International Relations and Mobility Program at the Graz University of Technology for assisting me with the grant application process.

This work was financially supported, in part, by generous contributions to Texas A&M University by Tommie E. and Carolyn S. Lohman as well as by a grant from the NIH

(HL086418). I also thank Dr. E. Wilson at the Texas A&M Health Science Center for maintaining the ApoE-/- colony and Dr. Y.U. Lee and Mr. J. Ferruzzi at Yale University for overseeing the initial histological preparation of the samples.

Finally, I want to thank the Austrian Marshall Plan Foundation for their generous funding which supported my Visiting Research Appointment at Yale University.

PAPER TITLE PAGE

Roles of Thrombus and Collagen Remodeling in Intramural Healing of Dissecting Aortic Aneurysms

A.J. Schriefl[1], M.J. Collins[2], J.S. Wilson[3], D.M. Pierce[1], G.A. Holzapfel[1], L.E. Niklason[4,5], J.D. Humphrey[3,5]

[1]Institute of Biomechanics
Graz University of Technology, Graz, Austria

[2]Department of Biomedical Engineering
Texas A&M University, College Station, TX, USA

[3]Department of Biomedical Engineering
Yale University, New Haven, CT, USA

[4]Department of Anesthesiology and [5]Vascular Biology and Therapeutic Program, Yale School of Medicine, New Haven, CT USA

ABSTRACT

Fibrillar collagen endows the normal aortic wall with significant stiffness and strength and similarly plays important roles in many disease processes. For example, because of the marked loss of elastic fibers and functional smooth cells in aortic aneurysms, collagen plays a particularly important role in controlling the dilatation of these lesions and governing their rupture potential. Recent findings now suggest that collagen remodeling may also play an important role in intramural healing following dissection of both arteries and aneurysms. To explore this possibility further, we identified and correlated regions of intramural thrombus and newly synthesized fibrillar collagen in a well-established mouse model of dissecting aortic aneurysms. Our findings suggest that intramural thrombus that is isolated from free-flowing blood creates a permissive environment for the synthesis of fibrillar collagen that, albeit initially less dense and organized, likely protects that region of the dissected wall from subsequent expansion of the dissection or rupture.

Keywords: thrombosis, glycosaminoglycans, collagen remodeling, rupture, thoracic aneurysm

INTRODUCTION

Thoracic aortic aneurysms (TAAs) and abdominal aortic aneurysms (AAAs) are responsible for significant morbidity and mortality, with younger individuals (< 60 years old) affected more by the former and older individuals (>70 years old) increasingly affected more by the latter in our aging society. Despite differences in etiology and natural history, fundamental mechanisms are shared at these two locations, including loss of elastin, apoptosis of smooth muscle, inflammation, and remodeling of collagen (Sakalihasan et al., 2005; Milewicz et al., 2008). There is a continuing need, however, for an increased understanding of the biochemomechanical conditions that lead to dilatation, dissection, and rupture (Vorp, 2007; Humphrey and Taylor, 2008). Motivated largely by the difficulty of collecting sufficient longitudinal information on lesion morphology, histology, cell biology, and biomechanical properties in humans, various animal models have been developed to study aortic aneurysms (cf. Daughtery and Cassis, 2004). Of the different models, continuous subcutaneous infusion of angiotensin-II (ANG-II) in the mouse has emerged as the most commonly used method to generate aortic aneurysms (e.g., Saraff et al., 2003; Barisione et al., 2006; Satoh et al., 2008; Lou et al., 2009; Tieu et al., 2009; Cao et al., 2010; Rush et al., 2010; Goergen et al., 2011; Rateri et al., 2011; Trachet et al., 2011). Via these and many similar studies, it appears that these lesions initiate following an accumulation of macrophages within the media, which produce cytokines and proteases that lead to degradation, dissection, and dilatation of the wall. Hence, although these lesions occur primarily in the suprarenal (i.e., abdominal) aorta, they exhibit some features that are more common to TAAs than to

AAAs in humans. Regardless of localization, for the purposes herein, lesions arising from the infusion of ANG-II provide an excellent model of a dissecting aortic aneurysm, including development of an intramural thrombus and possible subsequent healing of the dissected wall.

Notwithstanding the availability of significant information on the histology and cell biology associated with the ANG-II mouse model of dissecting aneurysms (cf. Daugherty et al., 2011 and references therein), little attention has been directed towards the turnover of fibrillar collagens and possible roles played therein by intramural and intraluminal thrombus. Because of the marked loss of elastic fibers and functional smooth muscle cells within the aneurysmal wall, fibrillar collagens play particularly important mechanical roles in controlling the rate of enlargement and governing the rupture-potential (Humphrey and Holzapfel, 2012). In particular, given that collagen is very stiff when straight (with an elastic modulus on the order of 1 GPa), vascular distensibility depends largely on the degree of undulation of the collagen fibers as well as on their density, fiber diameter, interactions with other matrix proteins and glycoproteins, and cross-linking (Humphrey, 2002). In this paper, we examine for the first time the waviness and density of fibrillar collagens at different locations within serial cross-sections along the length of dissecting aortic aneurysms that developed due to a 28-day infusion of ANG-II, with particular attention to the conversion of intramural thrombus to fibrillar collagen within this time-frame.

METHODS

Animal Model. All animal protocols were approved by the Texas A&M University Institutional Animal Care and Use Committee. Following other reports (e.g., Barisione et al., 2006), 8-week old male apolipoprotein null (ApoE-/-) mice were anesthetized with sodium pentobarbital and implanted subcutaneously in the mid-scapular region with an Alzet mini-osmotic pump (Durect Corp., CA). These pumps delivered ANG-II continuously at 1000 ng/kg/min. Following 28 days of treatment with ANG-II and maintenance on a normal diet, the mice were euthanized with an overdose of sodium pentobarbital. The suprarenal aorta was then isolated via a mid-line incision and photographed, large branches were ligated with 7-O silk, and the vessel was excised en-bloc. Following biomechanical testing (Genovese et al., 2012), the vessels were fixed in an unloaded configuration using a buffered 10% formalin.

Histology. Suprarenal aortas from five, 12-week old mice that developed significant aneurysms (> 1.5 fold increase in outer diameter) were cut into distal and proximal halves, embedded in paraffin (both halves in one block), and sectioned at five microns. Serial cross-sections were obtained for each half of the specimen at three axial locations separated by 880 microns, hence yielding 6 sets of axially located cross-sections per lesion. Supplemental Figure 1 gives an overview of the many resulting cross-sections for each vessel and thus illustrates the sectioning protocol. Sections were then stained with Verhoeff Van Gieson (VVG) to highlight elastin, picro-sirius red (PSR) to highlight fibrillar collagens, alcian blue to highlight glycosaminoglycans (GAGs), and Movat's pentachrome to identify fibrin, elastin, collagen, and glycosaminoglycans within a single section. All images were acquired

with an Olympus BX51TF microscope using an Olympus DP70 camera in combination with Olympus CellSens Dimension 1.4.1 software. In the case of the PSR-stained sections, images were acquired using appropriate polarizing optics and darkfield imaging; all other images were acquired using brightfield imaging. Magnification was typically set at 10-x or 20-x.

Image Analysis. As a measure of collagen waviness, we computed the "entropy" H from darkfield PSR-stained images collected from multiple locations within each cross-section. Straighter (more organized) fibers yielded lower values of entropy whereas increasingly wavy (more disorganized) fibers yielded higher values of entropy. Toward this end, each original darkfield image was first converted to an 8-bit (0 - 255) grayscale image that was then partitioned into five smaller images at each location to define multiple computational sub-domains for each analysis of waviness (Figure 1a). Each sub-domain was then divided into 25x25 pixel regions of interest (ROI), thus yielding n ROIs at each location of interest (Figure 1b). The collagen fiber organization within each ROI was then represented by a distribution function $f(x,y)$, where (x,y) defines a point in a 2-D real space. This distribution function was then transformed to Fourier space by performing a 2-D Fast Fourier Transformation, which yielded $\Im(f(x,y)) = F(u,v)$, where (u,v) is a point in Fourier space. The zero-frequency components were then shifted to the center and, finally, the 2-D power spectrum P of the Fourier Transform (FT) was obtained by multiplying the FT with its complex conjugate*, namely

$$P(u,v) = F(u,v) \cdot F^*(u,v). \quad (1)$$

The overall collagen fiber orientation within each ROI was then obtained by fitting a line through the center of the power spectrum in a least square sense (Xia and Elder,

2001). The orientation of the line provides the angle α as a measure of the overall fiber orientation for each ROI. All angles were then plotted as a histogram to yield a probability mass function $p(\alpha_i)$, which was normalized to $\sum_{i=1}^{n} p(\alpha_i) = 1$ (Figure 1c). Finally, the entropy was calculated from the probability mass function to yield a scalar measure of waviness of the collagen fibers, that is,

$$H = -\sum_{i=1}^{n} p(\alpha_i) \log_2 p(\alpha_i), \tag{2}$$

with n denoting the number of ROIs for each location of interest (Bayan et al., 2009).

To quantify the local density (or, "concentration") of the fibrillar collagen, we determined the area fraction of collagen present at multiple locations within each darkfield image. This quantification was performed on the same five computational sub-domains per location that were used for the analysis of waviness (cf. Figure 1a). This concentration was determined by calculating the ratio of colored pixels (representing the birefringent collagen fibers) to the black background for each domain. We emphasize that the term "concentration" is used loosely as a synonym for area fraction within a 2-D image and, therefore, it should not be confused with the biochemical term "concentration", as, for example, dry weight of collagen. All image analyses were performed using custom codes written in Matlab (MathWorks Inc., MA, USA). For isolating colors and applying color thresholds, we used ImageJ (U.S. National Institutes of Health, MD, USA).

RESULTS

AAAs were excised from five mice following 28 days of continuous infusion of ANG-II. Consistent with prior reports, these lesions tended to involve most of the suprarenal aorta and to be on the order of 2.5 mm in maximum outer diameter. In comparison, the normal outer diameter is on the order of 0.8 mm, hence ANG-II resulted in a remarkable 300+ percent localized increase consistent with the term aneurysm, which means "widening." Upon gross examination in a pilot study, it appeared that the true lumen was nearly preserved throughout much of the lesion, hence most of the gross dilatation resulted from an intramural accumulation of extracellular matrix material and thrombus (Figure 2). In some regions, however, a large parallel intramural cavity (presumably a false lumen) merged with the true lumen to form a much larger "merged" lumen.

Consistent with the gross observations (cf. Figure 2), serial histological sections revealed three primary distinctive formations in each of the five lesions (Figure 3a – c). Formation (a) consistently appeared within the region of maximum dilatation, which was typically near the center of the lesion, and was characterized by a ruptured media, that is, completely severed elastic fibers and smooth muscle at a single circumferential location within the media. This rupture allowed a large cavity, presumably a false lumen, to merge with the true lumen; this merged lumen is illustrated well in the VVG-stained cross-section shown as Figure 3a wherein the wavy elastic fibers appear black and the two arrows point to the site of medial rupture. Formation (b) typically appeared close to and on either side of the site of the merged lumen (i.e., just distal and proximal) and was characterized by an intact

lumen and parallel cavity that were separated by what appeared to be remodeled matrix (Figure 3b). Note that the true lumen in these regions was circumscribed by an intact media consisting of concentric elastic lamellae as expected of a normal aortic wall (cf. Collins et al., 2011). Formation (c) was found the farthest from the site of the merged lumen, again both distal and proximal, and was characterized by an intact true lumen and an intramural thrombus, which typically consisted of fibrin (Figure 3c) but in some cases GAGs and fibrillar collagen (Figure 4). Again, the true lumen was circumscribed by an apparently normal media. It should be noted that the black fragments visible on the outer perimeter in all cross-sections in Figure 3 are remnant India ink, which was used in mechanical tests that are reported elsewhere (Genovese et al., 2012). Furthermore, the symbols † and ‡ in Figure 3 denote locations where the waviness and concentration of fibrillar collagen were calculated, as described below.

Staining with PSR and Movat's pentachrome revealed interesting distributions of fibrillar collagen, fibrin, and GAGs (Figure 4a – f) in addition to the elastic fibers. Recall, therefore, that type I, or thick, collagen fibers appear bright red/orange whereas type III, or thin, collagen fibers appear less bright and more green/yellow in sections stained with PSR and viewed using polarized light. In contrast, collagen appears brownish/gray in sections stained with Movat's pentachrome while fibrin appears pink/red, GAGs light blue, and elastic fibers black. The thrombus in Figure 4a contained a small cavity that may have been exposed to flowing blood in vivo (i.e., it may have been a continuation of the aforementioned false lumen that merged with the true lumen in the central region; cf. Figure 3a). Interestingly, the thrombus surrounding this cavity stained a dark blue, see Figure 4a, which may indicate a region that was biologically more active due to its exposure to flowing blood. The

PSR-stained image of the corresponding area revealed collagen deposition in this region, with fibers organized parallel to the inner surface of the cavity (white arrows in Figure 4b). Figures 4c and 4d show regions of the same thrombus that were farther from the overall center of the lesion. The pink regions in the Movat's stain revealed an extensive asymmetric accumulation of fibrin containing little-to-no fibrillar collagen, which was confirmed by the lack of bright birefringence in the associated PSR image. Yet, at some locations near the expanding adventitia, brownish/light blue colors suggested the presence of small pockets of collagen and GAGs, which may mark regions where the thrombus began to remodel towards a collagenous tissue (white arrows in Figure 4d). Deposition of GAGs and collagen likely represent a wound healing type response, perhaps mediated by (myo)fibroblasts which migrated inwards from the adventitia. Figures 4e and 4f show sections that were the farthest from the center of the lesion while still exhibiting a dilated wall. Most of the pink coloration in the Movat's stain was gone, which indicated significantly less fibrin and thus intramural thrombus. Indeed, the extensive bluish/brown regions in Figure 4e suggest a remodeling of the thrombus to matrix rich in GAGs and collagen fibers, the latter of which was confirmed by the large amounts of fibrillar collagen visible in the darkfield image stained with PSR (Figure 4f). Given that it should take some time for fibroblasts to migrate from the adventitia into the thrombus and then produce significant amounts of collagen, these serial sections may suggest a "relative age" for the thrombus, that is, the time since the thrombus was either formed from or in contact with the flowing blood. Thus, one might speculate that the youngest thrombus (Figures 4a and 4b) occurred closest to the center of the lesion where the merged lumen could have continued to provide flowing blood (formation (a), Figure 3a), whereas the oldest region of the same

thrombus (Figures 4e and 4f) occurred farthest from the merged lumen and hence flowing blood.

To investigate further the possible colocalization of collagen and GAGs within a remodeling thrombus, we compared results from nearly sequential sections stained with PSR, Movat's pentachrome, and Alcian blue. Moreover, we used digital thresholding to focus individually on fibrin in the Movat's stain and GAGs in the Alcian blue stain. For example, Figures 5a – c reveal, on the one hand, the lack of fibrillar collagen in areas of "fresh" thrombus (cf. Figure 5a versus 5b), and on the other hand, the colocalization of GAGs and collagen (cf. Figure 5a versus 5c).

During our examinations of sections stained with PSR, we also noticed changes in collagen organization and appearance within the adventitia when comparing regions close to the true lumen (e.g., denoted by † in Figure 3) with those well away from the lumen (e.g., denoted by ‡ in Figure 3). Because of the tremendous asymmetric increase in diameter, collagen well away from the lumen must necessarily have remodeled (that is, collagen can only extend on the order of 10% once straight, yet some portions of the adventitia farthest from the lumen must have elongated on the order of 300% during the 28-day period of study). Figure 6 shows two representative darkfield images that highlight representative observed differences in collagen organization between locations † and ‡. Quantification of differences in collagen waviness and concentration at both locations for all three formations (a: merged lumen, b: lumen and cavity, c: lumen and intramural thrombus in Figure 3) are shown in Figure 7. Figures 7a (waviness) and 7b (concentration) display mean differences relative to an assumed nearly normal location as well as the corresponding standard errors of the mean. Comparisons between locations ‡ and † in the adventitia are given by dark gray bars (formations a

– c_1). In contrast, comparisons between collagen within a remodeled intramural thrombus and the adventitial location † are given by the light gray bars (formation c_2). Zero denotes a waviness and concentration equivalent to that in the adventitia nearest the lumen (location †), which appears to be closest to normal. The waviness analysis (Figure 7a) revealed that the remodeled collagen fibers at location ‡ were always less wavy than the more normal collagen fibers at location †, which is reflected by the decrease in entropy (formations a – c_1). Conversely, remodeled collagen fibers within the intramural thrombus were significantly more disorganized than normal as reflected by the increased entropy (formation c_2). These objective quantitative findings were expected based on a visual assessment, as, for example, when comparing the collagen organization in Figure 6a (more normal adventitia) with Figure 8f (remodeled intramural thrombus).

Results for the concentration of collagen (Figure 7b) revealed a significant decrease in the remodeled adventitia compared to the normal adventitia (formations a – c_1). This finding was also consistent with our visual impression from Figure 6, wherein collagen appears more densely packed at location † compared to location ‡. The lowest concentration of collagen fibers was found in the remodeled intramural thrombus, formation c_2, although we emphasize that the specific value of the concentration depended on both the location within the thrombus and the remodeling time. We would expect higher collagen concentrations with increasing thrombus age/remodeling time.

To gain further insight into the remodeling within the intramural thrombus, consider higher magnification (60x objective) images from locations separated axially by 880 microns within the same thrombus that was shown in Figure 4 and stained with Movat's pentachrome or picro-sirius red (Figure 8). Panels a and b display what

we suggest was the youngest region of the thrombus, that is, closest to the center of the lesion; panels (c) and (d) display an older region farther from the center; and panels (e) and (f) display what appears to be the oldest region of the same thrombus, farthest from the center. The sequence of picro-sirius red stained images (b,c,f) highlighted the progressive increase in collagen concentration and fiber thickness (brighter red) with remodeling, or aging, of the thrombus. Note that the "holes" in the birefrigent images likely reveal locations of synthetic cells, although possibly caniculi (cf. Wang et al., 2001). Results from the Movat's stain (a,c,e) revealed the associated progressive decrease in fibrin (pink/red) with thrombus age, consistent with the sequential replacement of degraded fibrin with collagen within the older regions.

DISCUSSION

Angiotensin-II (ANG-II) is a potent vasopressor having pluripotent activity. For example, systemic increases of ANG-II can cause vasoconstriction throughout the arterial tree, and thus increased systemic blood pressure; conversely, local increases of ANG-II within the arterial wall can lead to the increased production of diverse chemokines, cytokines, and proteases, which lead to significant localized remodeling of the wall. Although hypertension is generally considered to be a risk factor for human aneurysms and dissections, Cassis et al. (2009) showed that ANG-II generates dissecting suprarenal aneurysms in mice independent of blood pressure. Rather, it is the macrophages and other inflammatory cells that are recruited to the media and adventitia that play key roles in the development of these lesions (Tieu et al., 2009). Towards this end, note that one of the chemokines stimulated by angiotensin-II is monocyte chemoattractant protein 1 (or, MCP-1), which facilitates the recruitment of monocytes / macrophages to the media.

Although aortic lesions resulting from subcutaneous infusion of ANG-II in the mouse are typically suggested to model certain aspects of AAAs, these aneurysms seldom dissect in humans. In contrast, the present findings were consistent with the early report by Saraff et al. (2003) that ANG-II induced aneurysms in the mouse arise following an aortic dissection. For this reason, this animal model may be a better model of some aspects of TAAs, which often dissect and are similarly not understood well biomechanically. Nevertheless, a detailed study of histological and mechanical characteristics of this mouse model will increase our general understanding of the initiation and propagation of dissecting aneurysms.

Consistent with prior reports (cf. Daugherty et al., 2011), we found that the dissection presented as prototypically different formations along the axial direction (cf. Figures 2 and 3): a central region wherein medial elastin was completely fragmented and the true lumen merged with a false lumen; regions distal and proximal to the central region wherein the media was intact but there existed a large intramural cavity (false lumen) without thrombus; and regions farther distal and proximal to the central region wherein the media was intact but the intramural cavity was filled with either thrombus or remodeled thrombus consisting largely of GAGs and collagen. Little prior attention has been directed toward the potential remodeling of the intramural thrombus, however. Toward this end, it is interesting to note that clinical observations in patients having a dissecting TAA suggest that a patent false lumen may be a potential risk factor for continued aortic enlargement and a poor long-term outcome, but a partially thrombosed false lumen may be of even greater concern (Bode-Janisch et al., 2011; Clough et al., 2011). In contrast, a fully thrombosed false lumen may be protective, serving as a first step in "aortic wall healing and remodeling after repair" (Song et al., 2011). The present observations support the hypothesis that a thrombus isolated from flowing blood may allow an invasion of (myo)fibroblasts to replace the degrading fibrin with fibrillar collagens (cf. Irniger, 1963; Fineschi et al., 2009; Karsaj and Humphrey, 2010), which could potentially strengthen the wall and protect it from possible further dissection or rupture, at least within that region. Indeed, this hypothesis is consistent with the tacit assumption in the treatment of intracranial saccular aneurysms with clot-promoting coils. In this case, it is hoped that the intra-saccular thrombosis will become isolated from the bloodstream via re-endothelialization at the orifice of the lesion, thus allowing subsequent conversion of the thrombus to collagenous tissue by

invading myofibroblasts (Lee et al., 2007). What appears to be vital, therefore, is that the intramural or intraluminal clot be isolated from flowing blood, which of course can serve as a replenishing source of platelets, leukocytes and erythrocytes, fibrinogen (and thus fibrin), plasminogen (and thus plasmin), and so forth.

Whereas it is possible for a coil-induced thrombus in a treated intracranial saccular aneurysm having a narrow re-endothelialized neck to be isolated completely from the flowing blood, it is unlikely that an intraluminal thrombus in a true aneurysm (e.g., human AAAs) can ever be isolated. In contrast, much of the intramural thrombus within a false lumen in a dissected artery could become isolated from the flowing blood even if the "ends" of the thrombus are never so isolated. In this case, as in the case of the coiled intracranial aneurysm (cf. Lee et al., 2007), it is reasonable to expect that (myo)fibroblasts will invade and remodel the thrombus provided that there is sufficient oxygenation and modest levels of cells and biomolecules that arise from the blood – thrombus interface (cf. Houard et al., 2007; Folkesson et al., 2011). Our findings support this possibility.

The present findings do not provide any further information on possible reasons why a partially thrombosed dissection may be more susceptible to further dissection or rupture, however. There was no indication of local adverse remodeling or failure of the wall / remnant adventitia in regions containing the fibrin-rich thrombus. Indeed, it appears that if the aortic wall ruptures in this mouse model, it tends to do so early in the development of the dissection (generally 4-10 days following the initiation of ANG-II infusion; Barisone et al., 2006), perhaps during the period when all or most of the thrombus is newly formed. We focused herein on later developments, 28 days following the initiation of ANG-II.

Finally, we suggest a possible scenario (Figure 9) that is consistent with our histological observations, that is, the existence of three distinct formations (cf. Figures 2 and 3) in each of our five vessels and the different stages of thrombus remodeling therein. Figure 9a shows the possible initiation of an intramural delamination (due, in part, to the medial accumulation of macrophages; Daughtery et al., 2011), followed by a possible propagation of this delamination in Figure 9b (due to wall stresses exceeding local inter-lamellar strength) that leads to a medial dissection and a subsequent localized transmural tear that establishes communication with the lumen. Intramural pressures caused by the blood could propagate the dissection and initiate associated growth and remodeling processes within the remaining intramural constituents, leading to the observed dramatic increase in vessel circumference and formation of an intramural thrombus. Figure 9c illustrates a longitudinal section as a possible scenario for an advanced, 28-day dissecting aneurysm (cf. Figure 3 in Cao et al., 2010). Panels 9d – f show how the longitudinal section of Figure 9c might appear in typical histological cross-sections, which match the three formations we observed in all five lesions (cf. Figures 2 and 3). Additionally, relative differences in the age of the thrombus (i.e., time since it was in contact with flowing blood) can be explained using this scenario. The youngest region of the thrombus would occur at the center of the aneurysm, where it is exposed to the blood stream via the ruptured the intimal-medial layer. The oldest regions of thrombus would be farthest from the center of the lesion and not directly exposed to blood; this would allow more time for myofibroblasts to enter the intramural thrombus from the adventitia and to start the remodeling process (see Figure 4 and 8).

In summary, we have presented new observations related to collagen remodeling within dissecting aneurysms that arise in the most commonly employed mouse model of aortic aneurysms. The rapidly expanding adventitia clearly undergoes rapid remodeling, but so too the intramural thrombus in regions well separated from the flowing blood. Given that remodeling of thrombus to collagenous tissue represents a favorable wound healing response, effort should be directed toward understanding and promoting such remodeling in arterial dissections.

REFERENCES

Barisione C, Charnigo R, Howatt DA, Moorleghen JJ, Rateri DL, Daugherty A (2006) Rapid dilatation of the abdominal aorta during infusion of angiotensin II detected by noninvasive high-frequency ultrasound. J Vasc Surg 44: 372-376.

Bayan C, Levitt JM, Miller E, Kaplan D, Georgakoudi I (2009) Fully automated, quantitative, noninvasive assessment of collagen fiber content and organization in thick collagen gels. J Appl Phys 105:102042.

Bode-Janisch S, Schnidt A, Gunter D, Stuhrmann M, Fieguth A (2011) Aortic dissecting aneurysm – histopathological findings. Forensic Sci Intern (in press).

Cao RY, St. Amand T, Ford MD, Piomelli U, Funk CD (2010) The murine angiotensin II-induced abdominal aortic aneurysm model: rupture risk and inflammatory progression patterns. Front Pharmacol 1:9.

Cassis LA, Gupta M, Thayer S, Zhang Z, Charnigo R, Howatt DA, Rateri DL, Daugherty A (2009) Ang II infusion promotes abdominal aortic aneurysms independent of increased blood pressure in hypercholesterolemic mice. Am J Path 296: H1660-1665.

Clough RE, Hussain T, Uribe S, Greil GF, Razavi R, Taylor PR, Schaeffter T, Waltham M (2011) A new method for quantification of false lumen thrombosis in aortic dissection using magnetic resonance imaging and a blood pool contrast agent. J Vasc Surg (in press).

Collins MJ, Bersi M, Wilson E, Humphrey JD (2011a) Mechanical properties of suprarenal and infrarenal abdominal aorta: Implications for mouse models of aneurysms. Med Phys Engr (in press).

Daughtery A, Cassis LA (2004) Mouse models of abdominal aortic aneurysms. Arterioscler Thromb Vasc Biol 24: 429-434.

Daugherty A, Cassis LA, Lu H (2011) Complex pathologies of angiotensin-II-induced abdominal aortic aneurysms. J Zhejiang Univ-Sci B 12: 624-628.

Deng GG, Martin-McNulty B, Sukovich DA, Freay A, Halks-Miller M, Thinnes T, Loskutoff DJ, Carmeliet P, Doyle WP, Wang YX (2003) Urokinase-type plasminogen activator plays a critical role in angiotensin II-induced abdominal aortic aneurysm. Circ Res 92: 510-517.

Elefteriades JA, Farkas EA (2010) Thoracic aortic aneurysm. JACC 55: 841-857.

Fineschi V, Turillazzi E, Neri M, Pomara C, Riezzo I (2009) Histological age determination of venous thrombosis: A neglected forensic task in fatal pulmonary thrombo-embolism. Forensic Sci Intern 186: 22-28.

Folkesson M, Silveira A, Eriksson P, Swendenborg J (2011) Protease activity in the multi-layered intra-luminal thrombus of abdominal aortic aneurysms. Atherosclerosis (in press)

Genovese K, Collins MJ, Lee YU, Humphrey JD (2012) Regional finite strains in a murine angiotensin II model of dissecting aortic aneurysms. Cardiovasc Engr Tech (submitted).

Georgen CJ, Azuma J, Barr KN, Magdefessel L, Kallop DY, Gogineni A, Grewall A, Weimer RM, Connolly AJ, Dalman RL, Taylor CA, Tsao PS, Greve JM (2011) Influences of aortic motion and curvature on vessel expansion in murine experimental aneurysms. Arterioscl Thromb Vasc Biol 31: 270-279.

Houard X, Rouzet F, Touat Z, Philippe M, Dominguez M, Fontaine V, Sarda-Mantel L, Meulemans A, Le Guludec D, Meilhac O, Michel J-B (2007) Topology of the fibrinolytic

system within the mural thrombus of human abdominal aortic aneurysms. J Path 212: 20-28.

Humphrey JD (2002) Cardiovascular Solid Mechanics: Cells, Tissues, and Organs. Springer, NY.

Humphrey JD, Taylor CA (2008) Intracranial and abdominal aortic aneurysms: Similarities, differences, and need for a new class of computational models. Ann Rev Biomed Engr 10: 221-246.

Humphrey JD, Holzapfel GA (2012) Mechanics, mechanobiology, and modeling of human abdominal aorta and aneurysms. J Biomech (accepted).

Inoue N, Muramatsu M, Jin D, Takai S, Hayashi T, Katayama H, Kitaura Y, Tamai H, Miyazaki M (2009) Involvement of vascular angiotensin II forming enzymes in the progression of aortic abdominal aneurysms in angiotensin II infused ApoE-deficient mice. J Atheroscler Thromb 16: 165-171.

Irniger W (1963) Histologische altersbestimmung von thrombosen and embilien. Virchows Arch Path Anat 336: 220-237.

Karsaj I, Humphrey JD (2010) Mathematical model of the evolving mechanical properties of intraluminal thrombus. Biorheology 46: 509-527.

Lee D, Yuki I, Murayama Y, Chiang A, Nishimura I, Vinters HV, Wang CJ, Nien Y-L, Ishii A, Wu BM, Vinuela F (2007) Thrombus organization and healing in the swine experimental aneurysm model. Part I. A histological and molecular analysis. J Neurosurg 107: 94-108.

Lou J, Fujikura K, Tyrie LS, Tilson MD, Konofagou EE (2009) Pulse wave imaging of normal and aneurysmal abdominal aortas in vivo. IEEE Trans Med Imag 28: 477-486.

Milewicz DM, Guo DC, Fadulu VT, Lafont AL, Papke CL, Inamoto S, Kwartler CS, Pannu H (2008) Genetic basis of thoracic aortic aneurysms and dissections: Focus on

smooth muscle cell contractile dysfunction. Annu Rev Genomics Human Genetics 9: 283-302.

Rateri DL, Howatt DA, Moorleghen JJ, Charnigo R, Cassis LA, Daugherty A (2011) Prolonged infusion of angiotensin II in apoE -/- mice promotes macrophage recruitment with continued expansion of abdominal aortic aneurysms. Am J Path (in press).

Rush C, Nyara M, Moxon JV, Trollope A, Cullen B, Golledge (2009) Whole genome expression analysis within the angiotensin II – apolipoprotein E deficient mouse model of abdominal aortic aneurysm. BMC Genomics 10: 298.

Sakalihasan N, Limet R, Defawe OD (2005) Abdominal aortic aneurysm. Lancet 365: 1577-1589.

Saraff K, Babamusta F, Cassis LA, Daugherty A (2003) Aortic dissection precedes formation of aneurysms and atherosclerosis in angiotensin-II infused, apolipoprotein E-deficient mice. Arterioscl Thromb Vasc Biol 23: 1621-1626.

Satoh K, Nigro P, Matoba T, O'Dell MR, Cui Z, Shi X, Mohan A, Yan C, Abe J-I, Illig KA, Berk BC (2009) Cyclophilin A enhances vascular oxidative stress and the development of angiotensin-II induced aneurysms. Nature Med 15: 649-656.

Tieu BC, Lee C, Sun H, LeJeune W, Recinos A, Ju X, Spratt H, Guo DC, Milewicz D, Tilton RG, Brasier AR (2009) An adventitial IL-6/MCP-1 amplification loop accelerates macrophage-mediated vascular inflammation leading to aortic dissection in mice. J Clin Invest 119: 3637-3651.

Trachet B, Renard M, De Santis G, Staelens S, De Backer J, Antiga L, Loeys B, Segers P (2011) An integrated framework to quantitatively link mouse-specific hemodynamics to aneurysm formation in angiotensin II-infused ApoE -/- mice. Annl Biomed Engr (in press).

Vorp DA (2007) Biomechanics of abdominal aortic aneurysm. J Biomech 40: 1887-1902.

Wang DHJ, Makaroun MS, Webster MW, Vorp DA (2002) Effect of intraluminal thrombus on wall stress in patient-specific models of abdominal aortic aneurysms. J Vasc Surg 36: 598-604.

Xia Y, Elder K (2001) Quantification of the graphical details of collagen fibrils in transmission electron micrographs. J Microsc 204: 3-16.

FIGURES

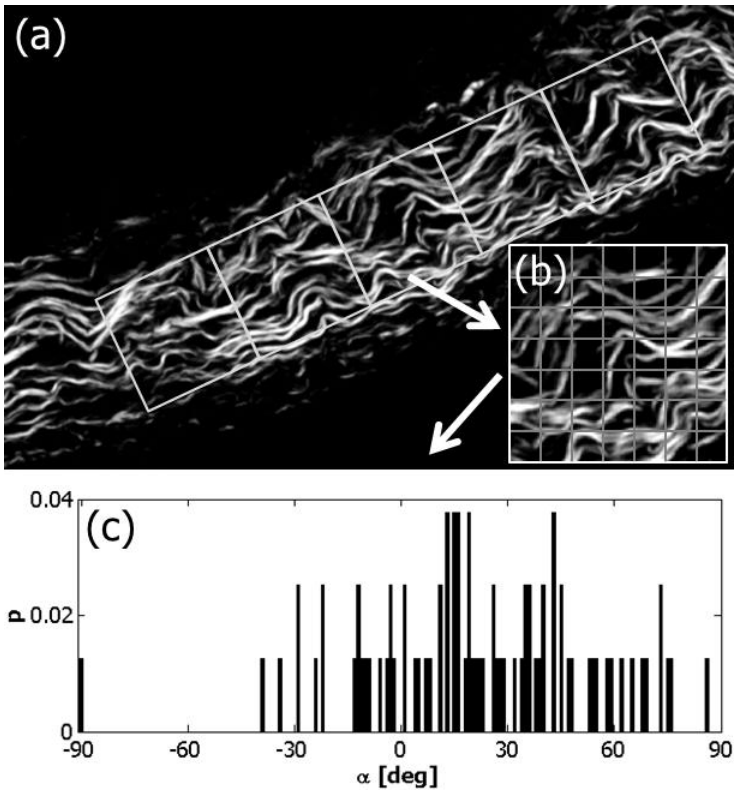

Figure 1: Schematic of the steps leading to the determination of the entropy H as a measure of collagen waviness. From the original image (a) five subsequent images from within the adventitia are created. (b) Each individual image is divided into 25x25 pixel ROIs. The overall fiber orientation *a* is determined for each ROI and plotted as a normalized histogram yielding the probability mass function p shown in (c). The entropy from this distribution is calculated according to Equation 2.

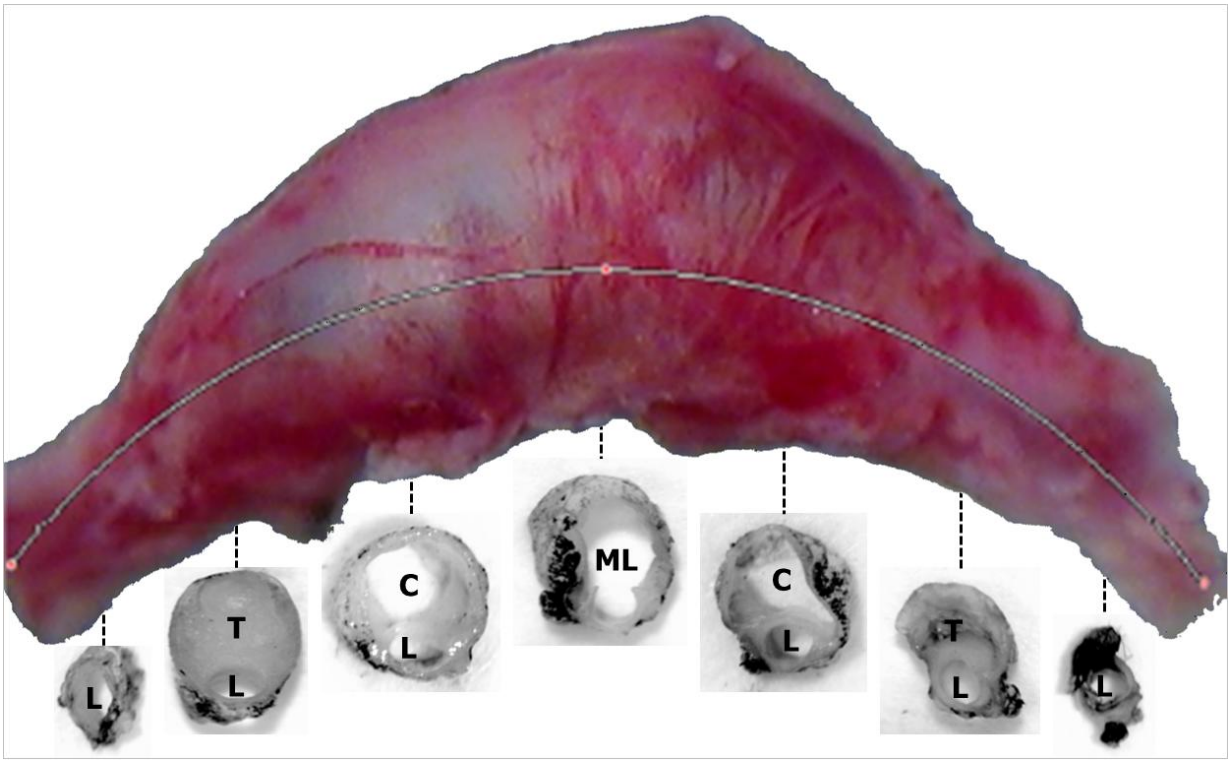

Figure 2: Photograph of a representative suprarenal aortic aneurysm that resulted following 28-days of a subcutaneous infusion of ANG-II. Shown, too, are reduced magnification photographs of cross-sections obtained from regions indicated by the dashed lines. L – lumen, T – thrombus, C – cavity, and ML – merged lumen (i.e., probable merging of the true lumen L with a false lumen / cavity. As noted below, the thrombus contained different constituents depending on position within the thrombus as well as its distance from the region of maximal dilatation.

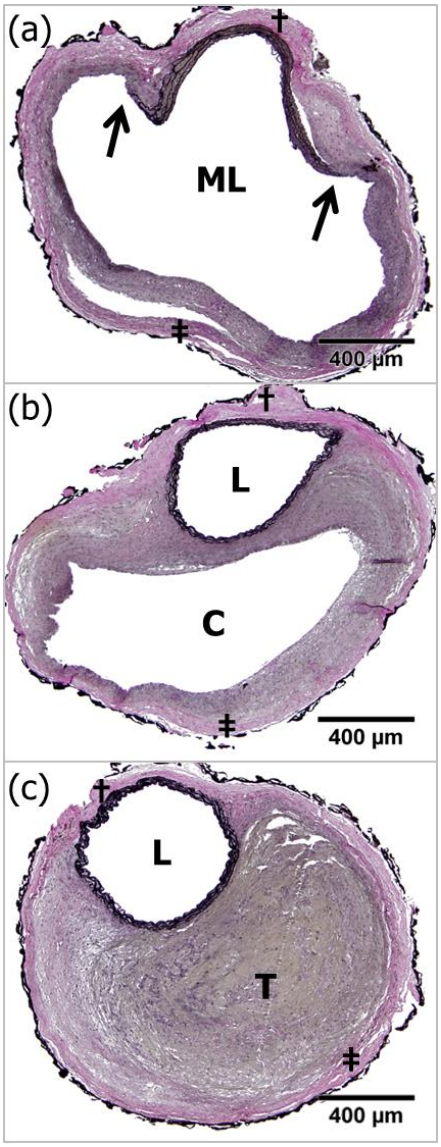

Figure 3: Representative VVG stained cross-sections of three distinct formations present within a dissecting aneurysm. Note: the wavy elastin within the normal media appears black in the stain. Note further: the black fragments that appear on the outermost perimeter are due to India ink which was used in mechanical tests that are reported elsewhere. Formation (a): merged lumen (ML). The arrows indicate the locations of the ruptured media. Formation (b): intact lumen (L) and cavity (C) separated by remodeled tissue. Formation (c): intact lumen (L) and intramural thrombus (T). † and ‡ denote the locations for subsequent analysis of the collagen fiber waviness.

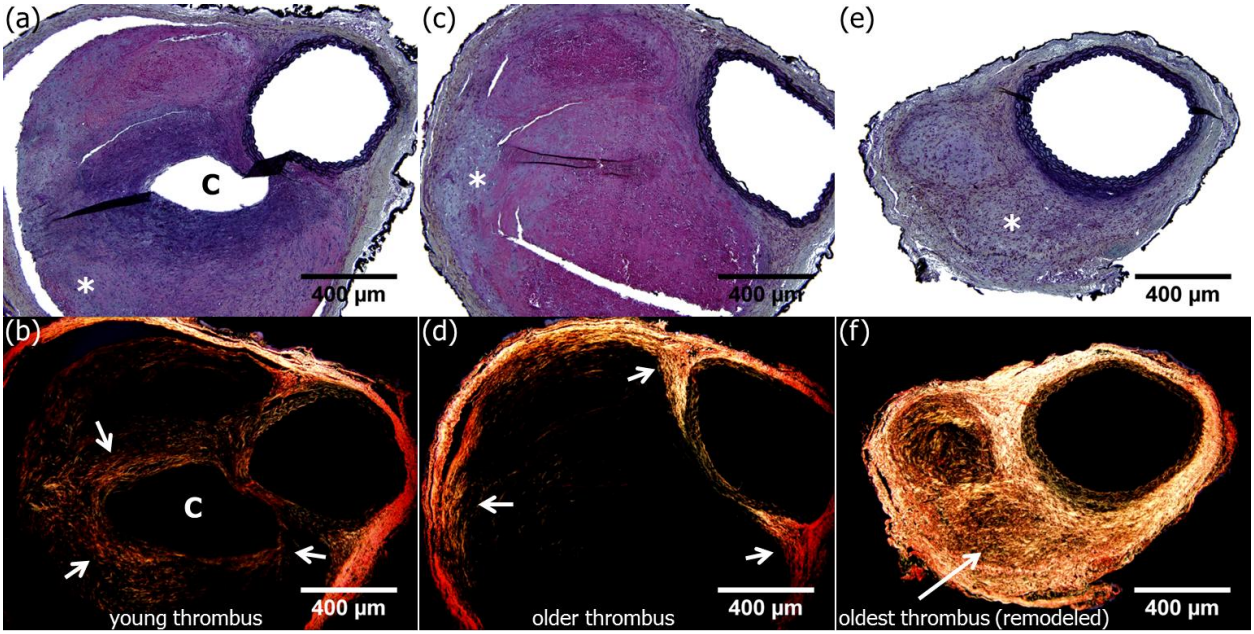

Figure 4: Movat's Pentachrome and corresponding Picrosirius red (PSR) stained images of aneurysmal cross-sections taken at three locations 880 microns apart. In the Movat's stain elastic fibers show black, fibrin appears as pink/red, GAGs appear as light blue and collagen appears as brownish/gray. In the PSR collagen type 1 or thicker fibers show as bright red/orange whereas thinner fibers appear less bright and show more green or yellow. (a) C denotes the cavity exposed to blood. The dark bluish area surrounding the cavity (*) marks the diffusion area for proteins, nutrients, white blood cells, etc., originating from the blood. It is an active area where collagen is laid down, indicated by arrows in (b). (c) Pink regions correspond to thrombotic material which has not been remodeled yet, hence no collagen is present in the same regions in (d). Brownish/light blue colors in (c), indicated by #, mark regions were remodeling of the thrombus started. An increased number of cells is visible, most likely (myo)fibroblast which migrated from the adventitia. Collagen is laid down, see arrows in (d). (e) Brownish/bluish colors correspond to remodeled thrombus (§). Lots of collagen is present, clearly visible in (f), while significantly less fibrin can be observed (lack of pink).

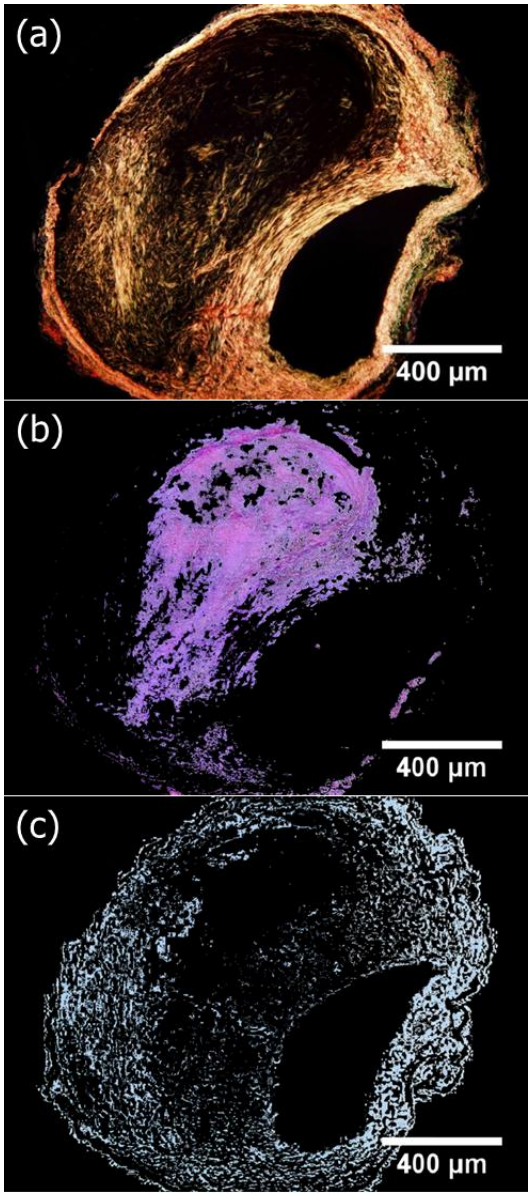

Figure 5: Isolated components of aneurysmal cross sections. (a) Dark field image of a Picrosirius red stained section showing collagen fibers, (b) thrombus isolated from a Movat's Pentachrome stained section, and (c) Glycosaminoglycans (GAGs) isolated from an Alcian Blue stained tissue section. Notice the lack of collagen in areas with thrombus present and the colocalization of collagen with GAGs. The single components in (b) and (c) were extracted from the original images using color thresholds in ImageJ.

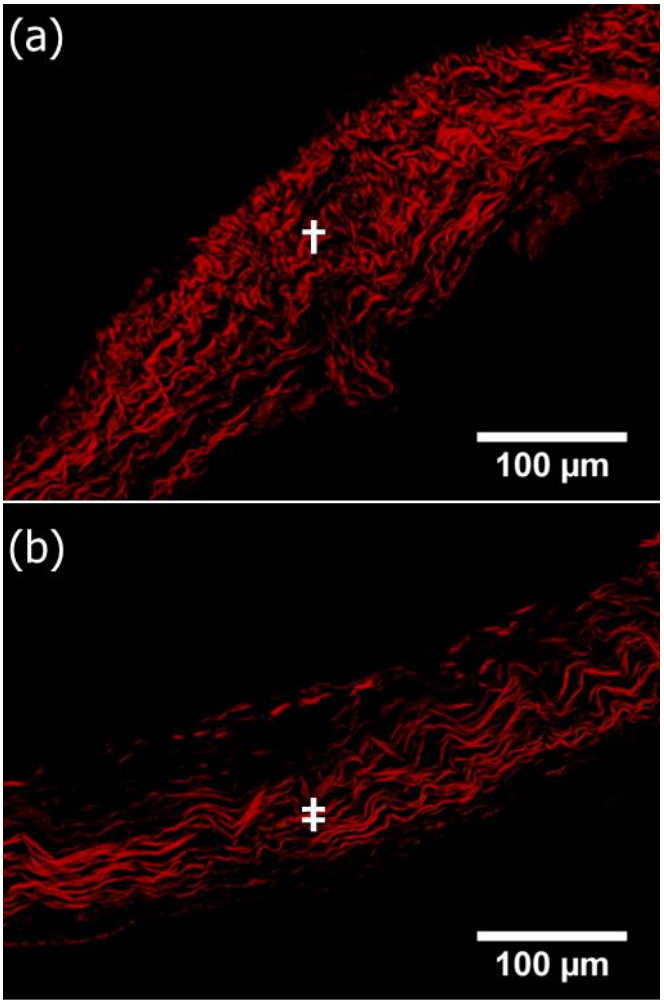

Figure 6: Representative dark field images of Picrosirius red stained sections showing collagen fibers in the adventitia at location † (healthy adventitia behind the lumen) versus location ‡ (remodeled collagen; opposite site of †). Both locations are defined in Figure 3.

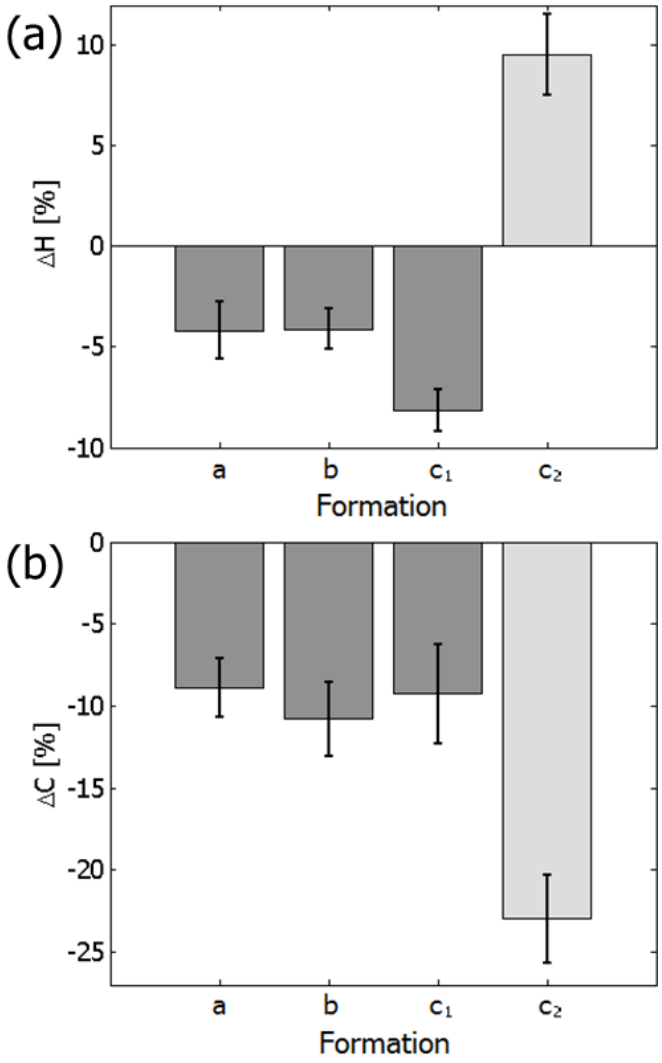

Figure 7: Both panels display averaged relative differences and corresponding standard error of the mean (SEM) in (a) collagen waviness and (b) collagen concentration for the three distinct cross-sectional formations present within an dissecting aneurysm. Formation a: merged lumen; formation b: lumen and cavity; formations c_1 and c_2: lumen and intramural thrombus. The dark gray bars (formations a – c_1) denote comparisons between locations ‡ and † in the adventitia. The light gray bars (formation c_2) denote comparisons between the collagen in a remodeled intramural thrombus (T) and adventitial collagen at location †. Zero denotes the collagen waviness and concentration of the healthy adventitia behind the lumen (location †). All formations and locations are defined in Figure 2.

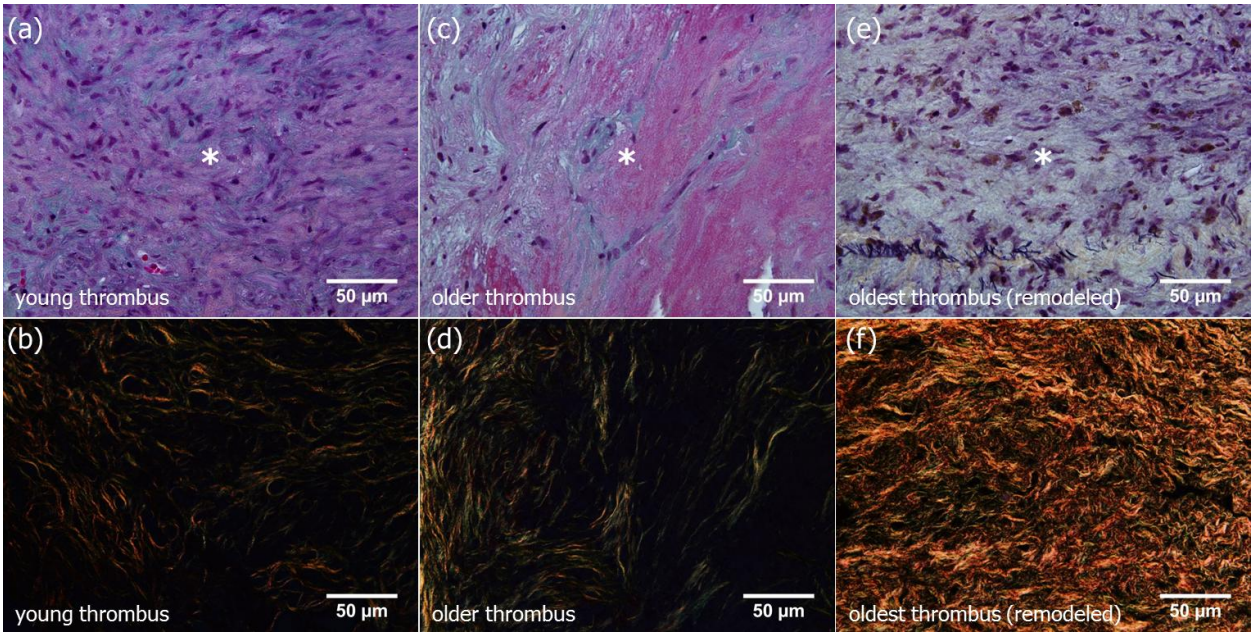

Figure 8: Movat's Pentachrome and corresponding Picrosirius red (PSR) stained close up images of the intramural thrombus shown in Figure 4. Figures (a) and (b) display the youngest thrombus closest to the center of the dissection aneurysm, (c) and (d) is from an older region of the same thrombus, further removed from the center, and (e) and (f) display the oldest region of this thrombus, furthest away from the center. The distance between the three regions is approximately 880 microns. The sequence of the PSR stained images (b,c,f) highlights the change in collagen structure and organization from originally laid down collagen surrounding cells and canaliculi (circular structures) in the young thrombus (b), to more fibrillar collagen structures in (d), to finally resulting in a fully (and rapidly) remodeled intramural thrombus in (f). The increase of collagen concentration in older regions of the thrombus is consistent with a decrease of fibrin, which appears pink/red in the Movat's stain. The entire remodeling process took place within three weeks.

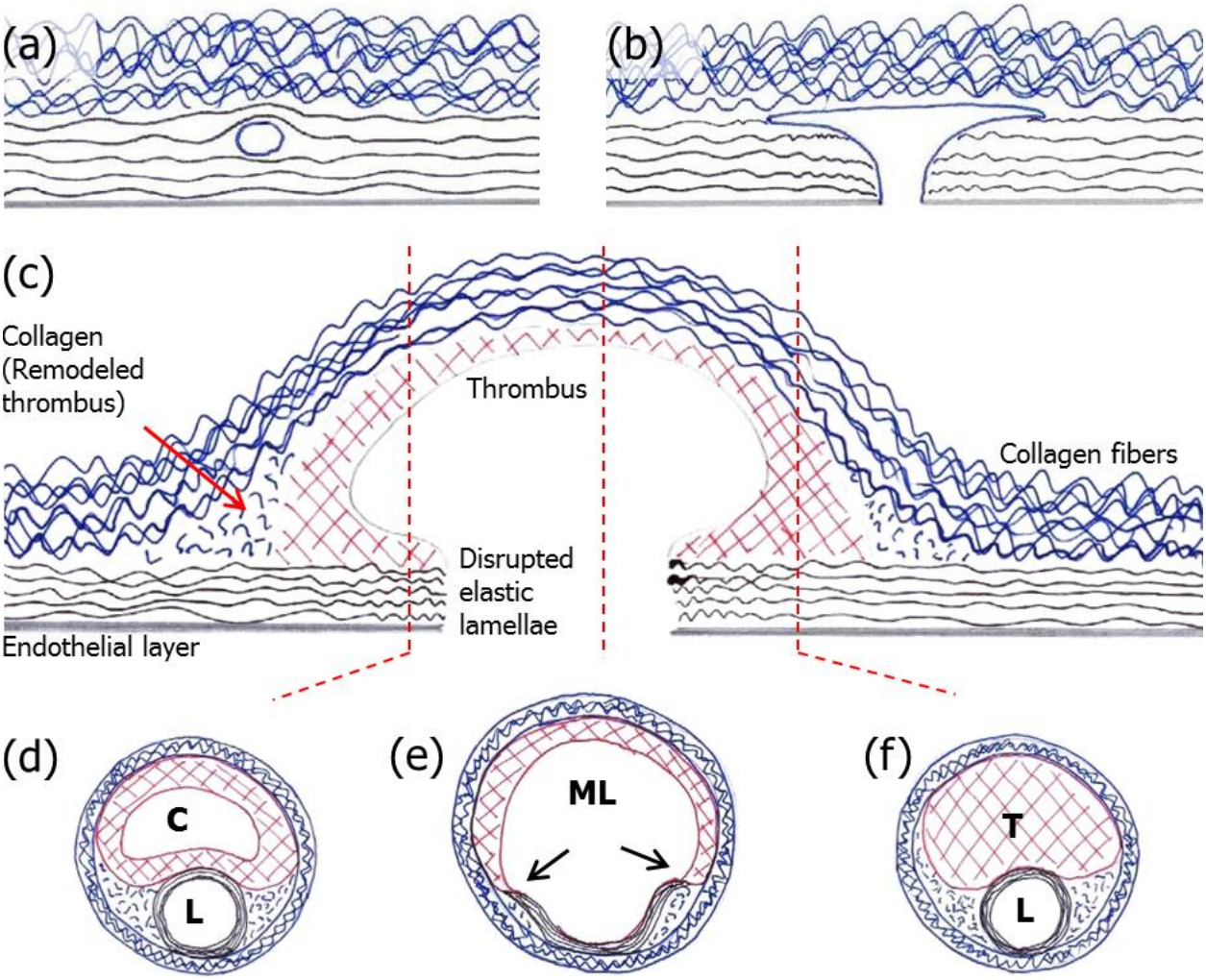

Figure 9: (a) Postulated mechanism for initiation of an intramural delamination. (b) Proposed propagation of this delamination creating a medial tear and subsequent communication with the blood stream. (c) Possible scenario for an advanced 28 day dissecting aneurysm. (d – f) show types of cross-sections that would be observed in a dissecting aneurysm as shown in Figure 2.

APPENDIX

SUPPLEMENTAL FIGURES

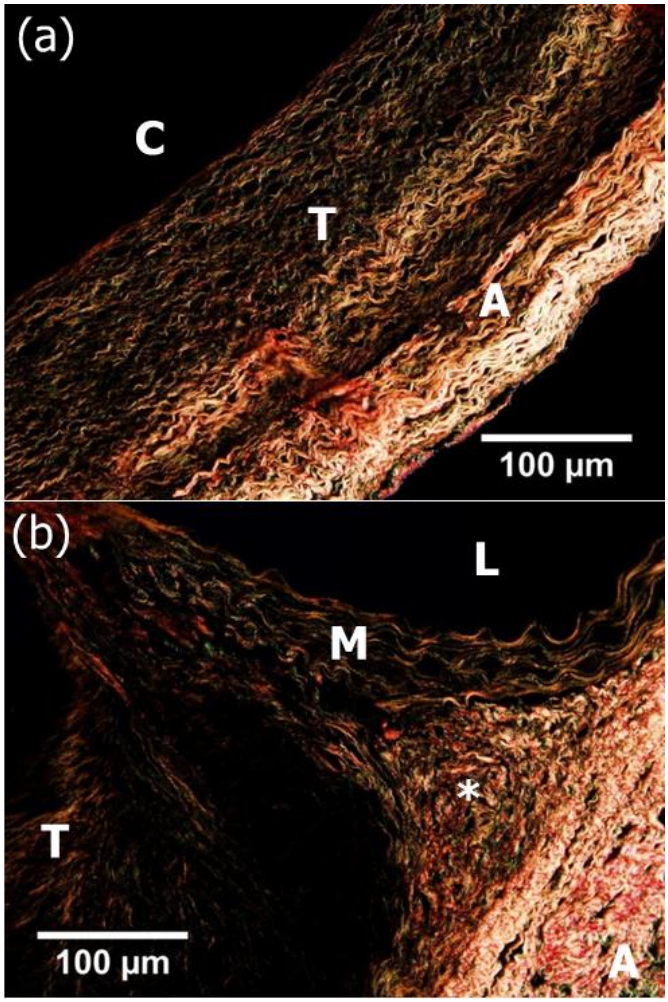

Supplemental Figure 1: Panel (a) is a representative image of layered collagen structures in the thrombus (T) and the adventitia (A). C denotes the cavity, as shown in Figure 3. Panel (b) highlights four different structures/formations of collagen within a few hundred microns. Note the differences in organization between the medial (M) and adventitial (A) collagen, the collagen in the remodeled thrombus (T), and the highly anisotropic collagen at the location marked with an asterisk (*).

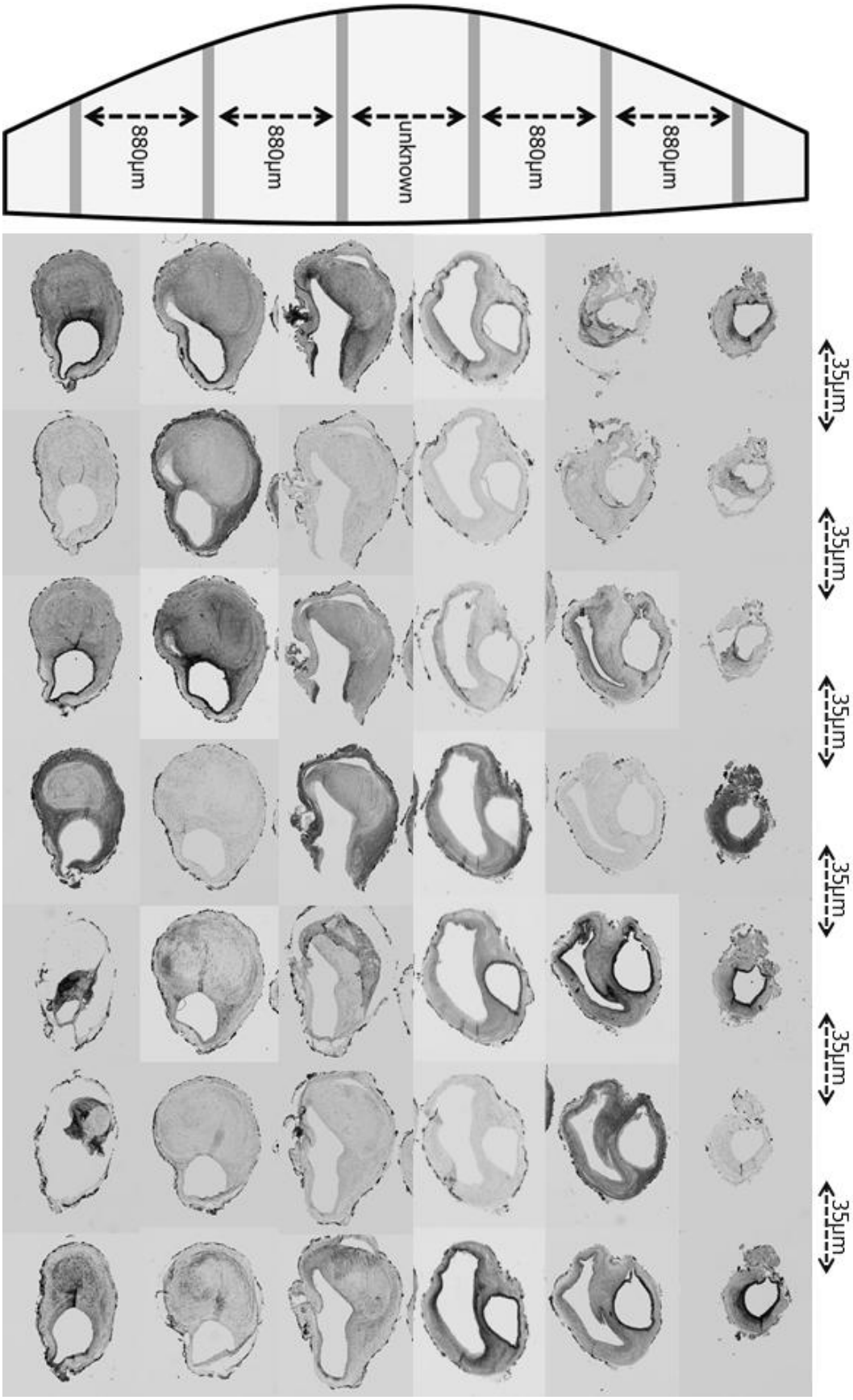

Supplemental Figure 2: Overview of cross-sections from vessel number 1.

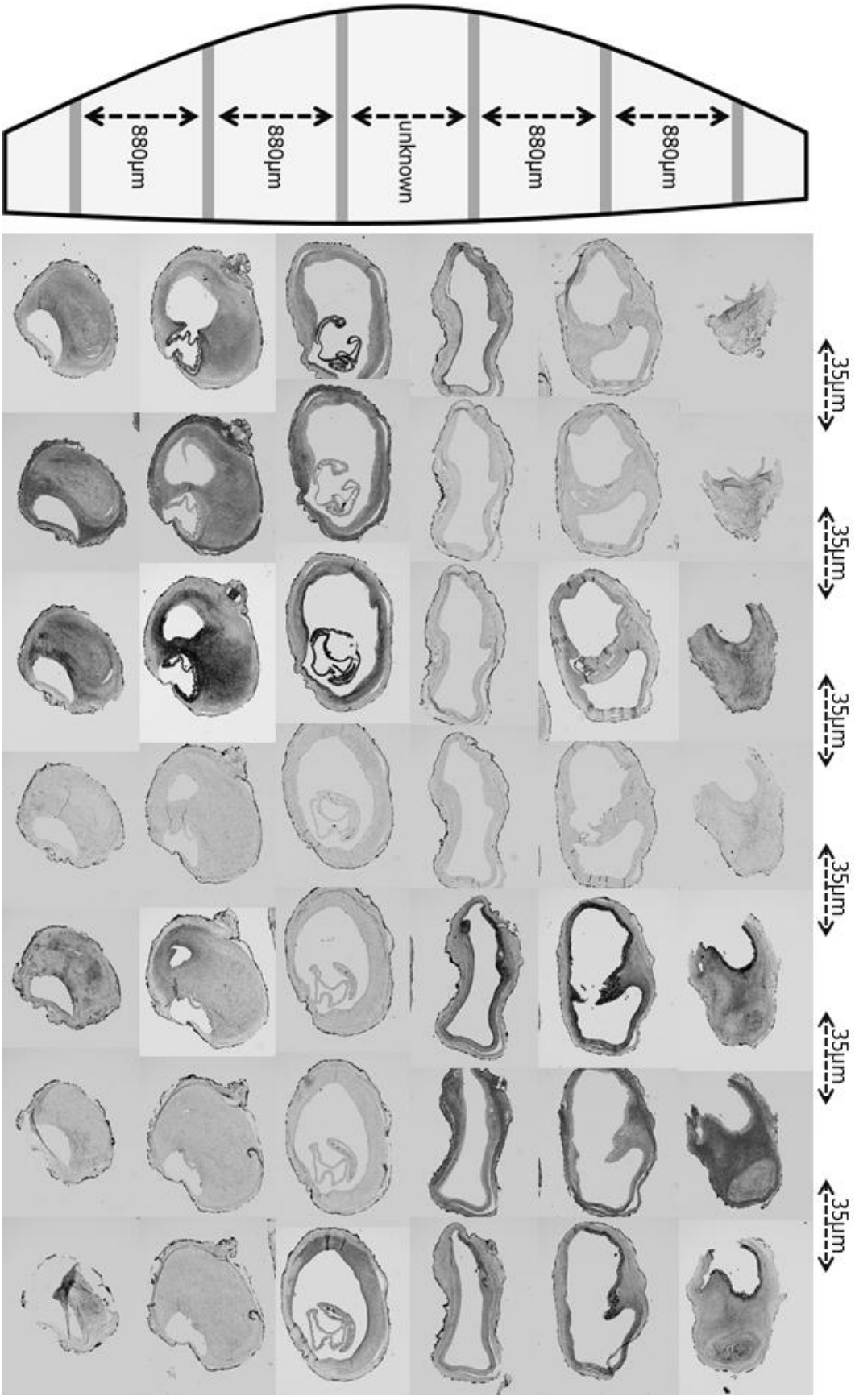

Supplemental Figure 3: Overview of cross-sections from vessel number 2.

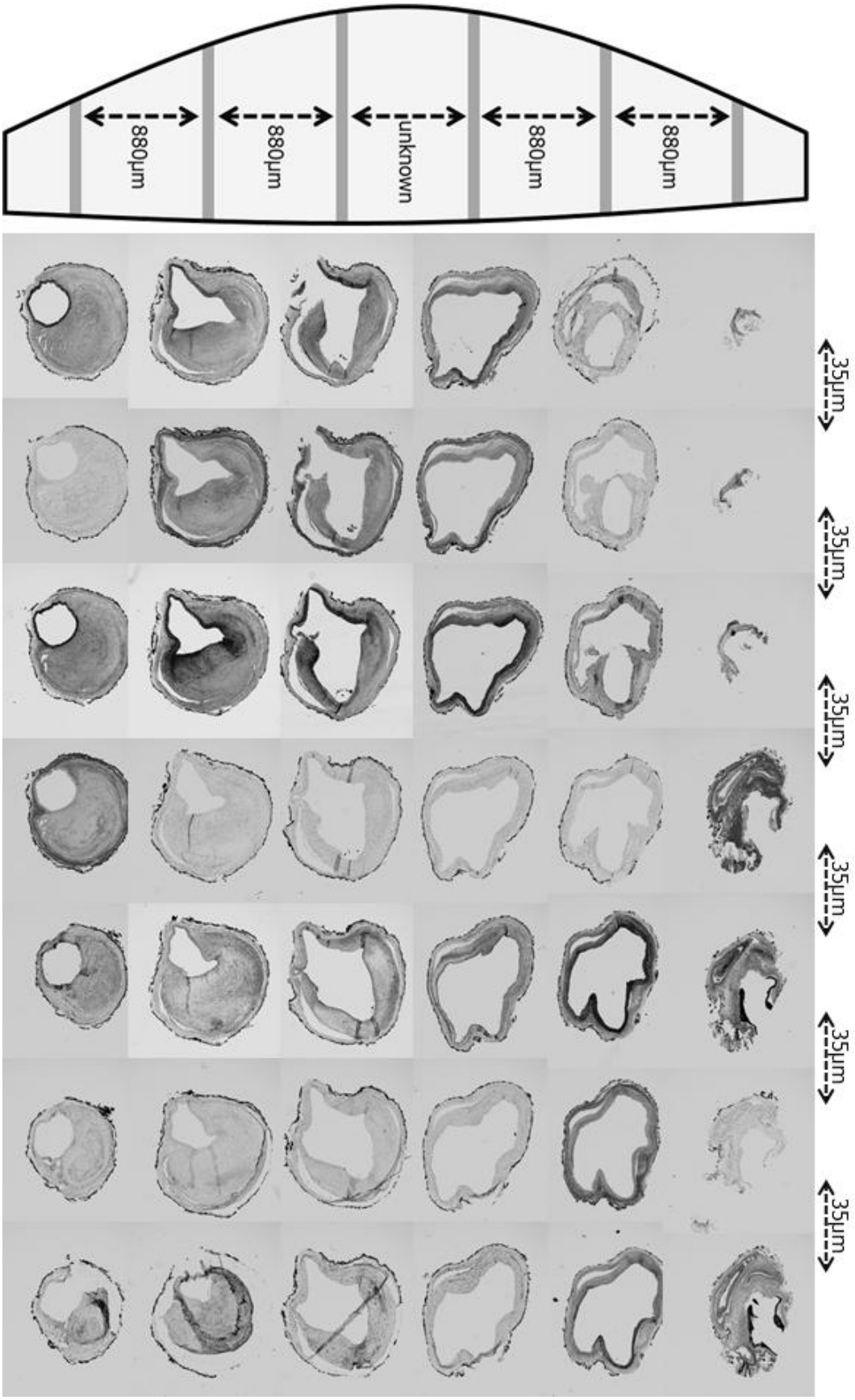

Supplemental Figure 4: Overview of cross-sections from vessel number 3.

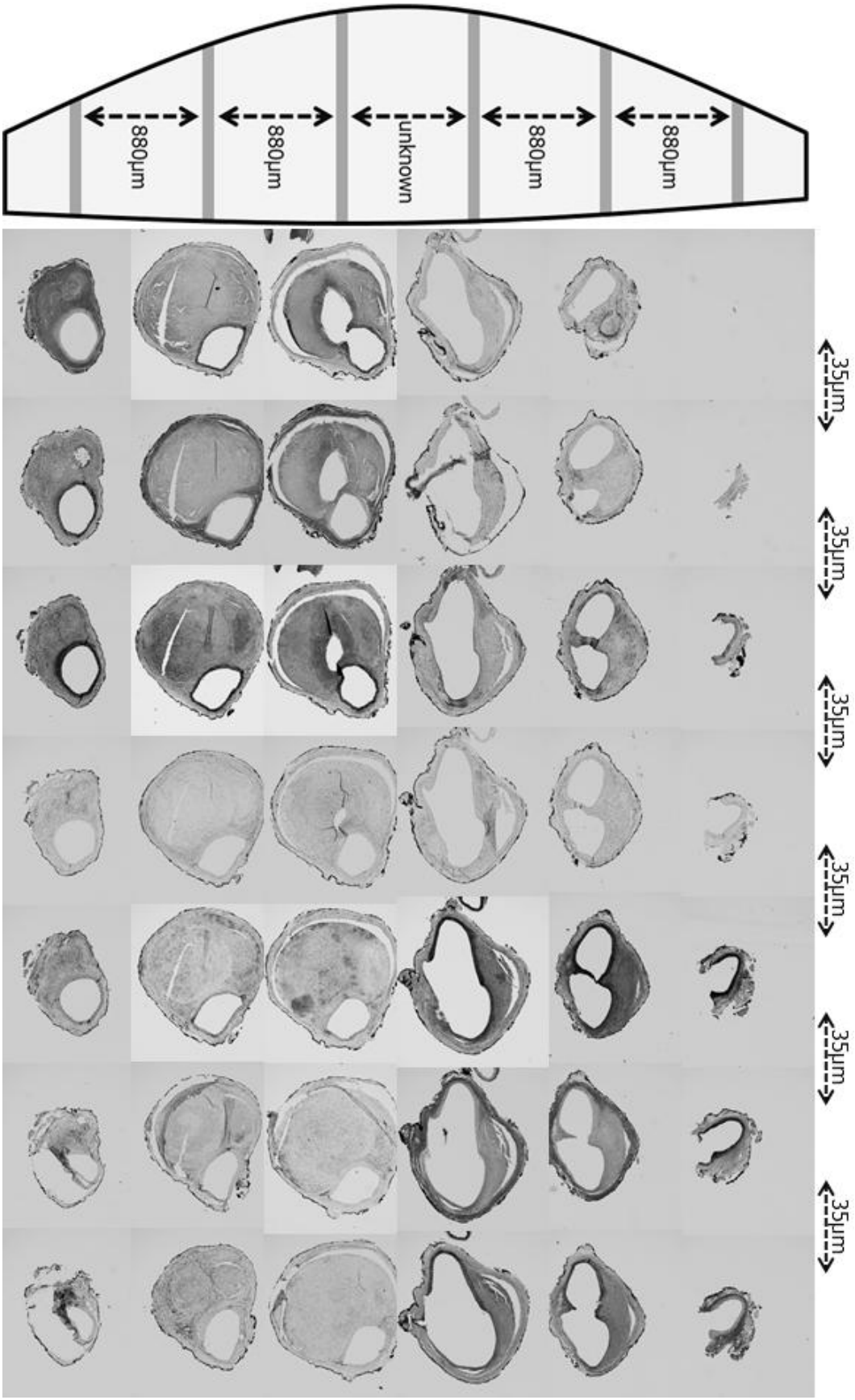

Supplemental Figure 5: Overview of cross-sections from vessel number 4.

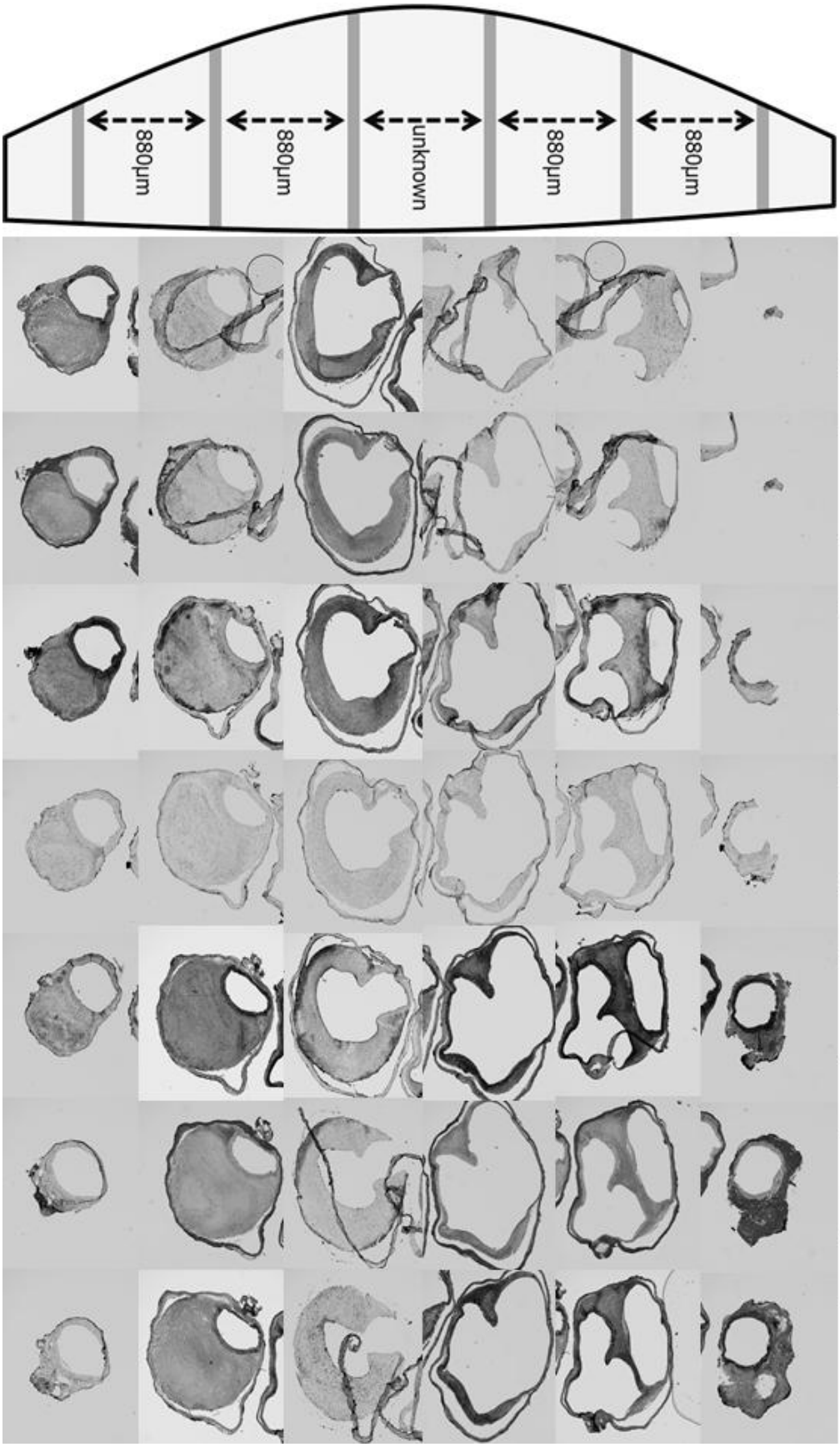

Supplemental Figure 6: Overview of cross-sections from vessel number 5.

CONVENTIONAL STAINS

Van Gieson's stain

A mixture of Picric Acid and Acid Fuchsin. It is the simplest method of differential staining of c and other connective tissue.

Common use	general staining
Nucleus	brownish black to black
Collagen (fibrous connective tissue)	pink or deep red
Muscle, Cytoplasm, RBC and Fibrin	yellow

Verhoeff-Van Gieson (VVG) stain

Also known as elastic-Van Gieson (EVG) stain. This is a combination of Verhoeff's elastic stain which is a hematoxylin stain containing ferric chloride and Wright's iodine solution and Van Gieson stain which contains acid fuchsin, picric acid, and hematoxylin. This stain stains elastic fibers blue-black to black, collagen pale red, other tissue elements yellow, and nuclei blue to black. Fine elastic fibrils may not be stained by this method.

Common use	elastic fibers
Elastic fibers	blue-black to black
Nucleus	blue to black
Collagen (fibrous connective tissue)	pale red
Other tissue elements	yellowish

Hematoxylin and eosin (HE) stain

The staining method involves the application of hemalum, which is a complex formed from aluminum ions and oxidized hematoxylin. The nuclear staining is followed by counterstaining with an aqueous or alcoholic solution of eosin Y, which colors eosinophilic other structures in various shades of red, pink and orange. The staining of nuclei by hemalum does not require the presence of DNA and is probably due to binding of the dye-metal complex to arginine-rich basic nucleoproteins such as histones.

Some structures do not stain well. Basal laminae need to be stained by PAS stain or some silver stains, if they have to be well visible. Reticular fibers also require silver stain. Hydrophobic structures also tend to remain clear; these are usually rich in fats, for example, adipocytes, myelin around neuron axons, and Golgi apparatus membranes.

Common use	general staining
Nucleus (bacteria, calcium)	blue
Collagen, muscle, cytoplasm	pink to red / blueish
Red blood cells	intensely red

Movat's Pentachrome Stain (Movat's stain)

Movat's Pentachrome stain is based on Alcian blue. It uses 5 different stains.

Common use	general staining, connective tissue
Elastic fibers, nucleus	black

Collagen, reticular fibers, bone	yellow
Ground substance (proteoglycans), mucin	blue
Muscle, cytoplasm	red
Fibrin	bright red

Masson's trichrome stain

A trichrome stain is a stain including three colored components. It is suited for distinguishing cells from surrounding connective tissue. The trichrome is applied by immersion of the fixated sample into Weigert's iron hematoxylin (a sequence of three solutions: ferric chloride in diluted hydrochloric acid, hematoxylin in 95% ethanol, and potassium ferricyanide solution alkalized by sodium borate; it is used to stain the nuclei), and then three different solutions Solution A, also called plasma stain, contains acid fuchsin, xylidine ponceau, glacial acetic acid, and distilled water. Other red acid dyes can be used, e.g. the Biebrich scarlet in Lillie's trichrome. Solution B contains phosphomolybdic acid in distilled water. Solution C, also called fiber stain, contains Light Green SF yellowish, or alternatively Fast Green FCF. It is used to stain collagen. If blue is preferred to green, methyl blue, water blue or aniline blue can be substituted.

Common use	Connective tissue
Nucleus	black/ dark red to purple
Connective tissue, collagen, bone	blue/green
Cytoplasm	light red/pink
Muscle fibers, keratin, red blood cell	red

Picrosirius Red (PSR)

The Picrosirius Red Stain binds specifically to collagen fibrils of varying diameter and can be used to distinguish collagen Type I (red to orange under polarized light) from Type III (greenish under polarized light). Collagenous structures of the mandible stain brilliant red. Unlike sections stained with hematoxylin and eosin alone, dentinal tubules, Sharpey's fibers and other structures can be seen clearly after using Picrosirius Red Stain procedure. Under polarized light, collagen fibers can be specifically identified and their orientation determined. Picrosirius Red staining is one of the best understood techniques of collagen histochemistry. The tissue fixation is not critical. The method is most frequently used on paraffin sections of objects fixed adequately in a neutral buffered formaldehyde solution, followed by polarized light microscopy.

Common use	Collagen
Collagen	red to orange birefringence for thicker fibers, greenish birefringence for thinner fibers

Alcian Blue

Alcian Blue is a phthalocyanine dye that contains copper which ultimately is responsible for the blue color. The dye stains acid mucopolysaccharides and glycosaminoglycans (GAGs), for which it is one of the most widely used cationic dyes. It is also used to look for goblet cells. It can be combined with H&E staining and van Gieson staining methods. It bonds by electrostatic forces with the negatively charged macromolecules. Gradual increases in the electrolyte concentration is used to wash

the bound dye. It allows to selectively identify neutral, sulphated, and phosphated mucopolysaccharides. Copper in the histology stain is what ultimately is responsible for the blue color. Excessive amounts of non-sulfated acidic mucosubstances are seen in mesotheliomas, certain amounts occur normally in blood vessel walls but increase in early lesions of atherosclerosis.

Common use	GAGs, mucopolysaccharides
GAGs, mucopolysaccharides, mucins	blue to bluish-green
Nucleus	pink/red
Cytoplasm	light pink

Safranin (Safranin O)

This is the classic counterstain in a Gram stain, staining Gram negative bacteria red in smears to contrast with the blue Gram positive organisms. For tissue sections it is useful as a red nuclear counterstain, and was popular at one time for staining cartilage metachromatically yellow, against red nuclei on a pink background. Safranin may also be used to give a yellow color to collagen. It can also be used for the detection of mucin and mast cell granules.

Common use	red nuclear counterstain (counterstain in a Gram stain)
Nucleus	red
Mucins (glycoconjugates)	orange/red
Cartilage, Collagen	yellow

Sudan stain

Sudan staining is the use of Sudan dyes to stain sudanophilic substances, usually lipids. Sudan lysochromes (Sudan II, Sudan III, Sudan IV, Oil Red O, and Sudan Black B) are used. Sudan dyes have high affinity to fats, therefore they are used to demonstrate triglycerides, lipids, and lipoproteins.

Oil Red O

Oil Red O (Solvent Red 27, Sudan Red 5B, C.I. 26125, C26H24N4O) is a lysochrome (fat-soluble dye) diazo dye used for staining of neutral triglycerides and lipids on frozen sections and some lipoproteins on paraffin sections. Oil Red O is one of the dyes used for Sudan staining. Similar dyes include Sudan III, Sudan IV, and Sudan Black B. The staining has to be performed on fresh samples or frozen sections, as alcohol fixation removes the lipids. Oil Red O has largely replaced Sudan III and Sudan IV as it is much deeper red in color, and consequently more clearly visible.

Common use	lipids and triglycerides on frozen sections
Nucleus	blue
Lipid	red to orange

Sudan blue

Sudan histology stains are used for staining of lipids and phospholipids. Examples of such histology stains are sudan blue, sudan black, sudan IV, and oil red O.

This staining uses Sudan dyes to stain sudanophilic substances, usually lipids. Sudan dyes have high affinity to fats, therefore they are used to demonstrate

triglycerides, lipids, and lipoproteins. While usually alcoholic solutions of Sudan dyes are used, pyridine solutions can be used in some situations as well. It is not commonly used anymore to stain lipids, instead Oil Red O is the preferred choice because it yields better results.

Hart's stain (Hart's elastic stain)

Hart's stain is used to stain elastic fibers and can be used on both, paraffin and frozen sections.

Common use	elastic fibers
Elastic fibers	blue to black
Collagen	red
Cytoplasm	yellow
Nuclei	blue

von Kossa Stain

Von Kossa staining is used for demonstrating deposits of calcium or calcium salt; it is not specific for the calcium ion itself. Silver ions are displaced from solution by carbonate or phosphate ions, due to their respective positions in the electrochemical series. The argentaffin reaction (see Masson Fontana), is photochemical in nature, and the activational energy is supplied from ultra violet light. Since the demonstrable forms of tissue carbonate or phosphate ions are invariably associated with calcium ions, the method may be considered as demonstrating sites of tissue calcium deposition. By selecting an appropriate counterstain, other tissue elements may be demonstrated as required, provided subsequent staining solutions used do

not remove the precipitated silver ions. The tissue sections can be formalin fixed, paraffin embedded or alcohol fixed frozen sections.

Common use	calcium staining
Calcium sites	black
Collagen	red
Osteoid	red

IMMUNOHISTOCHEMICAL (IHC) STAINS

Anti-Actin, smooth muscle, clone ASM-1

α-Smooth Muscle Actin Antibody (ASM-1) represents an excellent marker for myogenic soft tissue tumors and **smooth muscle differentiation**. This antibody reacts with many types of smooth muscle cells, such as those present in vascular walls, intestinal muscularis mucosae and propria, myometrium, stroma of various tissues, and is also positive for myoepithelial cells of various glands, notably salivary and mammary gland. Myogenic soft tissues detected by ASM-1 include leiomyosarcomas, leiomyomas, and certain stromal cells surrounding infiltrating ductal carcinoma of the breast.

CD68 antibody stain

CD 68 is a glycoprotein which binds to low density lipoprotein, expressed on **macrophages**/monocytes. The equivalent in mouse is called macrosialin. Macrosialin is a heavily glycosylated transmembrane protein of 87-115kD, which is specifically expressed by tissue macrophages, Langerhans cells and at low levels by dendritic cells. Macrosialin is the murine homologue of the human macrophage glycoprotein CD68, both are members of the lysosomal-associated membrane protein (lamp) family which are located predominantly within the cells and can be detected by flow cytometry using cell permeablisation. MCA1957 does detect surface macrosialin at low levels in resident mouse peritoneal macrophages which can be enhanced with thioglycollate stimulation.

CD45 Antibody staining

Cluster of Differentiation 45 (CD45) antibody staining is more general than Cleaved Caspase-3 (see below). The A20 antibody reacts with CD45 (Leukocyte Common Antigen) on all leukocytes of mouse strains expressing the CD45.1 alloantigen (e.g., RIII, SJL/J, STS/A, DA). This alloantigen was originally named Ly-5.2, and this was the designation at the time that the antibody was characterized. The designation was later changed from Ly-5.2 to Ly-5.1 to conform with the convention that the alloantigen designations be assigned to the C57BL/6 strain. mAb A20 does not react with leukocytes of most other mouse strains, which express the CD45.2 alloantigen. CD45 is a member of the Protein Tyrosine Phosphatase (PTP) family: Its intracellular (COOH-terminal) region contains two PTP catalytic domains, and the extracellular region is highly variable due to alternative splicing of exons (designated A, B, and C, respectively), plus differing levels of glycosylation. **The CD45 isoforms detected in the mouse are cell type-, maturation-, and activation state-specific**. The CD45 isoforms play complex roles in T-cell and B-cell antigen receptor signal transduction. The A20 antibody has been reported to inhibit some responses of B cells, from mice expressing the CD45.1 alloantigen, to antigens5 and LPS

Cleaved Caspase-3 antibody stain

Caspase-3 (CPP-32, Apoptain, Yama, SCA-1) is one of the key executioners of **apoptosis**, as it is either partially or totally responsible for the proteolytic cleavage of many key proteins such as the nuclear enzyme poly (ADPribose) polymerase (PARP). Activation of caspase-3 requires proteolytic processing of its inactive zymogen into activated p17 and p12 fragments. Cleavage of caspase-3 requires aspartic acid at the P1 position.

Caldesmon stain

Caldesmon binds calcium, calmodulin, tropomyosin and actin, and regulates smooth muscle contraction. H-caldesmon is its high molecular weight isoform, found in smooth muscle cells; l-caldesmon isoform is distributed in non-muscle cells. It is very useful to distinguish smooth muscle cells/lesions (positive) from myofibroblastic cells/lesions. Caldesmon stain also distinguishes uterine leiomyoma or leiomyosarcoma (positive) from endometrial stromal tumors (negative), but endometrial stromal tumors may have focal smooth muscle differentiation. It is sensitive and specific for epithelioid peritoneal mesothelioma (positive) versus ovarian serous carcinoma (negative) and epithelioid pleural mesothelioma (positive) versus pulmonary adenocarcinoma (negative).